Experimental and numerical study on rapid inflation process of air-launched balloon

PENG SUN   HAN CHENG
FEI LONG

ABSTRACT – REZUMAT

Experimental and numerical study on rapid inflation process of air-launched balloon

The rapid inflation process is the most important stage in the whole working process of rapid deployment of aerostat. However, it is difficult to reveal its mechanical mechanism by existing experimental and numerical methods and reasonably explain the damage and helium leakage during the inflation process. An air-launched balloon for rapid deployment was designed and manufactured, and the related ground steady inflation experiment was carried out in this work. Then, the rapid inflation process of the folded balloon was studied by using the Simplified Arbitrary Lagrangian-Eulerian (SALE) method. Here, the folded balloon model was obtained by the reverse folding method. The structure and flow field were described by Lagrangian elements, and the coupling between them was obtained by a contact algorithm. The numerical results were in good agreement with the experimental results. The numerical method in this work could obtain abundant information on the structure and flow field which couldn't be obtained by the experimental method. The change law of structure and flow field was obtained and the failure mechanism in the destructive experiment was explained. The numerical method proposed in this work could provide a reference for the material selection, gas source selection and structure optimization of the rapid deployment aerostat system.

Keywords: air-launched balloon, high strength fabric, inflation process, numerical method, rapid deployment

Studiu experimental și numeric asupra procesului de umflare rapidă a balonului lansat cu aer

Procesul de umflare rapidă este cea mai importantă etapă a întregului proces de desfășurare rapidă a aerostatului. Cu toate acestea, este dificil să se analizeze componenta sa mecanică prin metodele experimentale și numerice existente și să se explice în mod rezonabil daunele și scurgerile de heliu în timpul procesului de umflare. A fost proiectat și fabricat un balon lansat cu aer pentru desfășurare rapidă, iar experimentul aferent de umflare constantă la sol a fost prezentat în această lucrare. Apoi, procesul de umflare rapidă a balonului pliat a fost studiat folosind metoda Euler-Lagrange Arbitrară Simplificată (SALE). Aici, modelul balonului pliat a fost obținut prin metoda de pliere inversă. Structura și câmpul de curgere au fost descrise de elemente lagrangiene, iar cuplarea dintre ele a fost obținută printr-un algoritm de contact. Rezultatele numerice au fost în corelație cu rezultatele experimentale. Metoda numerică din această lucrare ar putea oferi informații multiple asupra structurii și câmpului de curgere, care nu au putut fi obținute prin metoda experimentală. S-a obținut legea de schimbare a structurii și a câmpului de curgere și a fost explicat mecanismul de defecțiune în experimentul distructiv. Metoda numerică propusă în această lucrare ar putea oferi o referință pentru selecția materialului, selecția sursei de gaz și optimizarea structurii sistemului aerostat cu desfășurare rapidă.

Cuvinte-cheie: balon lansat cu aer, țesătură de înaltă rezistență, proces de umflare, metodă numerică, desfășurare rapidă

INTRODUCTION

The traditional aerostats have many limitations, high risk in the launching process and long deployment time [1]. In some applications, especially in outer space exploration and military applications, traditional aerostats are not suitable. Therefore, the concept of rapid deployment aerostat was proposed. The rapid deployment aerostat system is first transported to the launch area by vehicles (aircraft, rocket, etc.). After the rapid deployment aerostat is launched, the parachute is used to decelerate. Then the folded aerostat is pulled out and inflated rapidly. Finally, the inflated aerostat separated from the parachute system. The rapid deployment aerostat was originally used for Venus's suspension detection in the 1960s

[2]. Subsequently, the Air Force Geophysics Laboratory (AFGL) started the development of the Air-Launched Balloon System (ALBS). The related research works mainly relied on a large number of ground tests and airdrop tests by different vehicles [3, 4] because the numerical simulation technology was not mature at that time. But the follow-up research progress has not been reported. With the increasing frequency of human activities to explore outer space, the rapid deployment of aerostats has once again attracted the attention of scholars, and the relevant research was restated gradually in the past decade [1].

Compared with the traditional aerostat, the most complicated stage of rapid deployment aerostat is the

rapid inflation in dropping. Due to the rarefied atmosphere at high altitude or in outer space, the parachute's deceleration effect is limited. The aerostat must be inflated rapidly to produce buoyancy. However, the nozzle velocity at the critical outgassing stage of the high-pressure helium gas source is about three times the air sound velocity. The huge impact velocity will make the aerostat deform and displace rapidly, and the displacement of the skin will change the direction of the gas source. While, this change will further aggravate the uncertainty of the internal flow field, and easily causes skin damage. Given the above-complicated engineering and science problems, the experiments are undoubtedly the most direct solution. However, the existing experiments only study the tearing performance of skin material [5], and it is difficult to obtain the internal flow field and the stress change of skin.

With the development of computer hardware and the maturity of numerical technology, numerical methods have gradually become an important research method. The representative works are as follows. Bessert proposed a fluid-structure coupling method based on potential flow theory to solve the static aeroelastic problem of airship [6]. Liu used the loose coupling method to realize the static aeroelastic analysis of airship respectively [7]. Zhang constructed an unsteady explicit dynamic fluid-structure coupling analysis framework and used this framework to study the relationship between vibration frequency and pressure difference of airship [8]. The above works focused on the static aeroelasticity, but few on the inflation process. Although the research objects were different, scholars also have proposed a variety of numerical models to study the inflation process of other inflatable fabrics. Stein proposed Computational Fluid Dynamics/ Mass Spring Damper (CFD/MSD) model [9]. The fabric was described by a series of mass points connected by spring and damper, so the stress change couldn't be calculated in this model. Tezduyar proposed the model of Deforming Spatial Domain/Stabilized Space-Time (DSD/SST) [10]. This method has high calculation accuracy based on body-fitted grid technology, but it is not suitable for inflation study of complicated folded fabrics. The Immersed Boundary Method (IBM) proposed by Peskin could be used in 2D and 3D fabric inflation process [11], but it is limited to a certain Reynolds number range. In addition, there are Ghost Fluid Method (GFM), Smoothed Particle Hydrodynamics/ Finite Element (SPH/FE), Arbitrary Lagrangian-Eulerian (ALE), Embedded Boundary Method (EBM) and other methods have also been used in fabrics inflation calculation [12–15]. However, most of these methods are used for a single infinite gas source (such as a fixed external wind field), and the effect of buoyance is not considered. So far, the works about rapid inflation of complicated folded rapid deployment aerostat are few.

To solve the above problems, an air-launched balloon used for rapid deployment was taken as the research object in this work. The SALE (Simplified Arbitrary Lagrangian-Eulerian) method based on multi-material fluid was used to calculate the rapid inflation process, and the corresponding ground inflation experiment was used to verify this numerical model. The change law of structure and flow field was analyzed. The method used in this work could provide references for the subsequent design and optimization of the rapid deployment aerostat.

MATHEMATICAL MODEL

There are a lot of irregular folds on the folded aerostat, so it is difficult to establish the body grid of the flow field. Here, the finite elements are used to describe the balloon and flow field. The biggest advantage of Lagrangian description is that it could accurately track the material boundary, which naturally satisfies the mass conservation. In addition, due to the short inflation time and the impermeability of the skin, the heat transfer between different materials was not considered in this work. Therefore, only the momentum equation needed to be considered:

$$\int_\Omega B_{lj} \sigma_{ji} \, d\Omega - \int_\Omega N_l \rho b_i \, d\Omega - \int_{\Gamma_{t_i}} N_l \bar{t}_i \, d\Gamma +$$
$$+ \delta_{ij} \int_\Omega N_l N_J \rho \, d\Omega v_{Ji} = 0 \qquad (1)$$

where B_{lj} is geometric matrix component, σ_{ji} – Cauchy stress component, N_l – shape function, ρ – density, b_i – body force component, $\bar{t}$ – surface force component, v_{Ji} – velocity component, δ_{ij} – Kronecker symbol, Ω – current configuration, Γ – current configuration boundary.

The central difference scheme was used for time discretization:

$$v^{n+\frac{1}{2}} = v^{n-\frac{1}{2}} + \Delta t^n M^{-1} (f^{\text{ext}}(d^n, t^n) - f^{\text{int}}(d^n, t^n)) =$$
$$= v^{n+\frac{1}{2}} + \Delta t^n M^{-1} f^n \qquad (2)$$

where M is mass matrix, d – node displacement and t – time.

The folded balloon model was established by reverse folding method [16] in this work, the quadrilateral or triangular high order elements would cause the initial distortion before inflation calculation. Therefore, the simplest 3-node element was used to discretize the structure. In addition, the structure presents small strain and large displacement in the inflation process. The Kirchhoff constitutive model (equation 3) was adopted in this work. Then the second Piola Kirchhoff (PK2) stress S was converted into Cauchy stress σ by equation 4 and used for explicit calculation:

$$\begin{Bmatrix} S_{11} \\ S_{22} \\ S_{12} \end{Bmatrix} = \frac{E}{(1+\upsilon)(1-2\upsilon)} \begin{bmatrix} 1-\upsilon & \upsilon & 0 \\ \upsilon & 1-\upsilon & 0 \\ 0 & 0 & \frac{1-2\upsilon}{2} \end{bmatrix} \begin{Bmatrix} E_{11} \\ E_{22} \\ E_{12} \end{Bmatrix} \qquad (3)$$

$$\sigma = J^{-1} F \cdot S \cdot F^{\mathrm{T}} \qquad (4)$$

where S_{ij} is PK2 stress component, E_{ij} – Green strain component, E – elastic modulus, υ – Poisson's ratio, J – Jacobian determinant and F – deformation gradient matrix.

However, the flow field based on the finite element description doesn't need the transformation between PK2 stress and Cauchy stress, and its constitutive equation and state equation are as follows:

$$\sigma_{ij} = \mu(v_{i,j} + v_{j,i}) - p\,\delta_{ij} \qquad (5)$$

$$p = (1 - \gamma)\rho\omega^{int} \qquad (6)$$

where μ is dynamic viscosity coefficient, p – pressure, γ – specific heat of gas and ω^{int} – internal energy per unit mass.

Both the structure and flow field were discretized by the finite element method in this work, and the fluid structure coupling could be understood as the contact between the two materials. Therefore, the transmission of coupling information could be realized by contact algorithm [14].

The disadvantage of flow field based on Lagrangian description is also obvious. The fluid constitutive model is different from the structure and the shear force will cause element distortion, which makes it impossible to continue the calculation. Therefore, it is necessary to re-construct the distorted grids and update the flow field in-formation (figure 1).
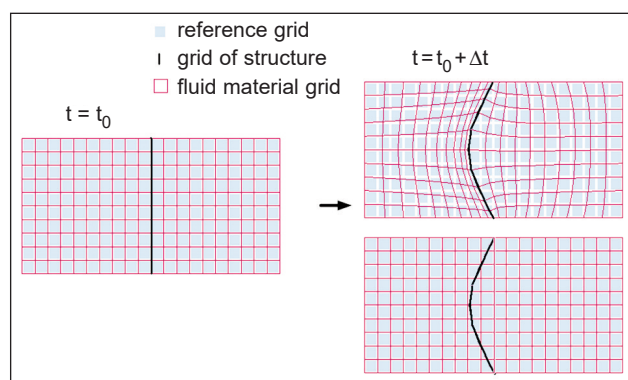

Fig. 1. Flow field reconstruction and information updating

The 4-node hexahedral grid is used to discretize the flow field (reference grid). At $t = t_0$, the fluid material grid based on Lagrangian description is consistent with the reference grid. Under the action of external force, the fluid material grid appears distortion. Then, the grid reconstruction is realized by solving Laplace differential equation.

The topological relationship between the fluid material grid and reference grid remains unchanged after grid reconstruction. The flux ϕ (mass, momentum and the other flow information) in the flow field is updated by solving equation 7:

$$\frac{\partial\phi}{\partial t} + \frac{\partial v_i\phi}{\partial x_i} \qquad (7)$$

where v_i is convective velocity in flow field. The discretization scheme of convection term is as follow.

$$\phi^{n+1}V^{n+1} = \phi^n V^n + \sum_{j=1}^{6} f_j^\phi \qquad (8)$$

Where V is volume of element and f_j^ϕ – flux form adjacent element. And the flux f_j^ϕ is obtained by

MUSCL (Monotone Upwind Schemes for Conservation Laws) Scheme [17].

CASE STUDY

The air-launched balloon used for rapid deployment was taken as the research object in this work. The diameter of this balloon is 1.425 m (figure 2). In order to prevent the balloon's damage during pulling out, a central reinforcing rope (1.425 m) connected the top and bottom of the balloon is added. The outer skin has no reinforcement layer to achieve lightweight of system, so the rapid inflation might cause skin damage. Therefore, an internal airbag around the charging valve is added and 10 gas outlets with a diameter of 0.02 m are evenly distributed on the internal airbag. Here, the internal airbag is made of polyethylene composite with high strength fabric. The material parameters are shown in table 1.
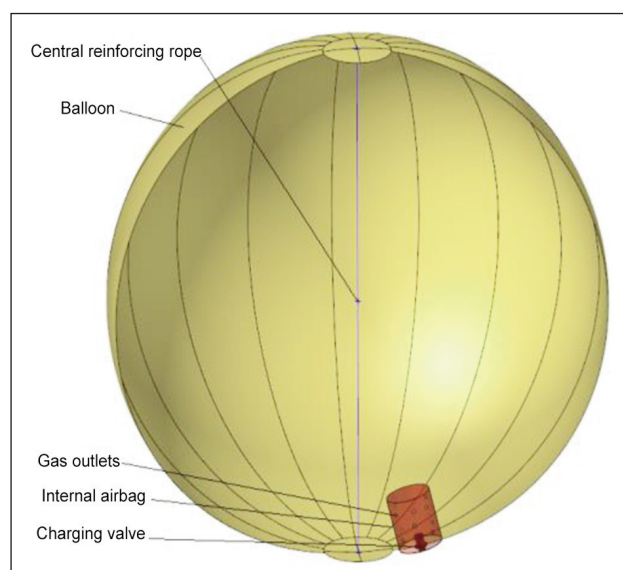

Fig. 2. Structure diagram of air-launched balloon

Table 1

MATERIAL PARAMETERS OF AIR-LAUNCHED BALLOON		
Parameter	**Outer skin (Type ZT1076)**	**Internal airbag (Type 3216LV)**
Elastic modulus (Pa)	4.4E8	9.8E9
Density (kg/m^2)	0.05	0.205
Thickness (m)	2E-4	2.2E-4
Poisson's ratio	0.3	0.35

In order to simulate the rapid inflation process during airdropping, the flexible constraints are adopted at the top and bottom of the balloon. Helium is charged into the balloon through the inflating tube. After the internal airbag is inflated rapidly, helium inflates into the balloon through the 10 gas outlets on the internal airbag (figure 2). The whole experiment was carried out at standard atmospheric pressure environment (figure 3), and the folded balloon was inflated with 0.1
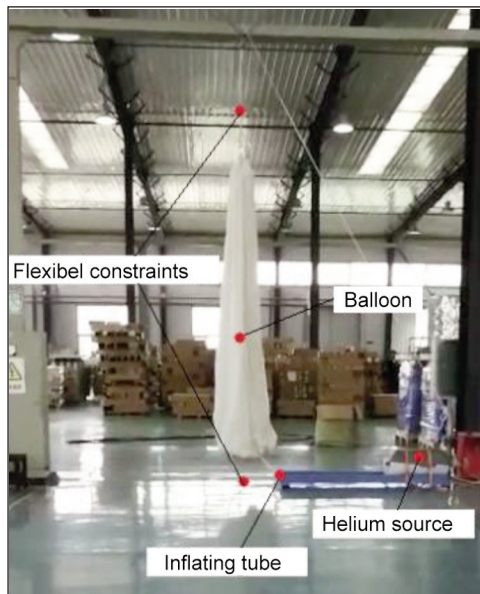
Fig. 3. Ground steady inflation experiment

Fig. 4. Complete fluid structure coupling model

kg/s steady flow for 20 seconds. The average temperature in the balloon was $-30°$.

It is very difficult to establish the folded balloon model as shown in figure 3 by using the traditional modeling method. Therefore, the reverse folding method [16] was used to obtain the final folded balloon model in this work. Here, the balloon is discretized by 3-node triangular elements (48,266), and the top and bottom of the balloon are fixed to replace the function of the central reinforcing rope. The area of charging valve's outlet and gas outlets on the internal airbag are very small. If these outlets are discretized by elements, the local element size and critical time step Δt_{crit} ($\Delta t_{crit} \leq \min(l_e/c_e)$, l_e is element's characteristic length, c_e – current wave velocity) will be too small and the amount of calculation will increase sharply in the explicit calculation. In order to solve this problem, the mass point is used to replace the whole charging valve and the point gas sources are used to replace the 10 gas outlets on the internal airbag. The hexahedral elements (308,705) are used to discretize the whole flow field, and the whole flow field is a cylinder with a height of 5.5 m and a diameter of 4.6 m. In order to simulate the buoyancy background, the flow field is divided into two parts. The outermost elements are flow field 1, and the rest are flow field 2. The upper surface hydrostatic pressure p_0 of the top elements of flow field 1 is defended as 1 atm, and that of the other elements of flow field 1 is defined as p_i ($p_i = p_0 + \rho_{air} \cdot g \cdot h_i$, h_i is the depth of the current element i, g is the acceleration of gravity). Finally, the elements of the balloon and flow field are assembled by interpenetration, and the complete fluid-structure coupling model is shown in figure 4.

The strength of the internal airbag is much greater than that of the outer skin (table 1). The previous strength experiments also proved that its strength was enough to meet the requirement. In addition, the
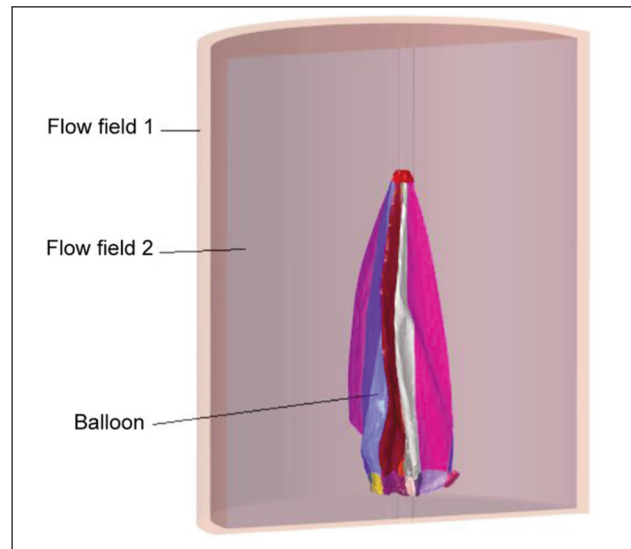
internal airbag was filled in a very short time and the main research focus of this work was rapid inflation process and the dynamic change of outer skin in this work. Therefore, the internal airbag didn't participate in the fluid structure coupling calculation, but only in the contact calculation with other structural parts. Here, an additional pressure with 1000 Pa was applied on the internal airbag to ensure the rapid expansion of the internal airbag and maintain the filled shape during inflation calculation. The point gas sources were defined on the nodes according to the design. While the charging valve (additional mass point) and the gas outlets (point gas sources) were used to define a vector to control the charging direction in this work (figure 5).
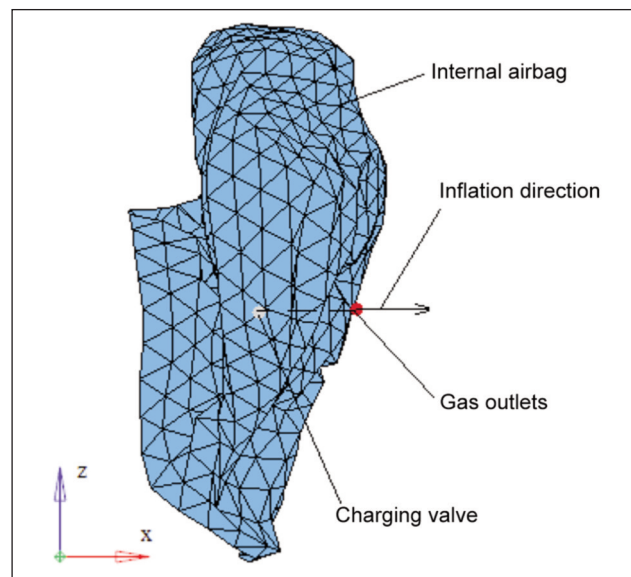

Fig. 5. Definition of inflation direction of gas outlets

RESULTS AND DISCUSSIONS

Figure 6 shows the shape change comparison of numerical results and experimental results. It could

be found that the two results are in good agreement. The whole rapid inflation process could be divided into three stages.

Initial inflation stage (0-2s): The shape change of balloon in this stage is the most violent during the whole inflation process. The bottom expands rapidly after helium is released from the point gas sources. Then helium flows to the balloon's top rapidly under the action of buoyancy. Because the internal airbag is on one side of the balloon, the shape change presents asymmetrical.

Middle inflation stage (2-6s): A large amount of helium gathers at the balloon's top, and the folds at the top part begin to expand gradually. The buoyancy overcomes the gravity of the balloon. The balloon begins to float and its shape gradually becomes symmetrical.

Final inflation stage (6-20s): After the top part is fully expanded, the balloon changes more stable. In this stage, the balloon is gradually filled from top to bottom. Finally, it forms the inflated shape shown in figure 6, *f*.
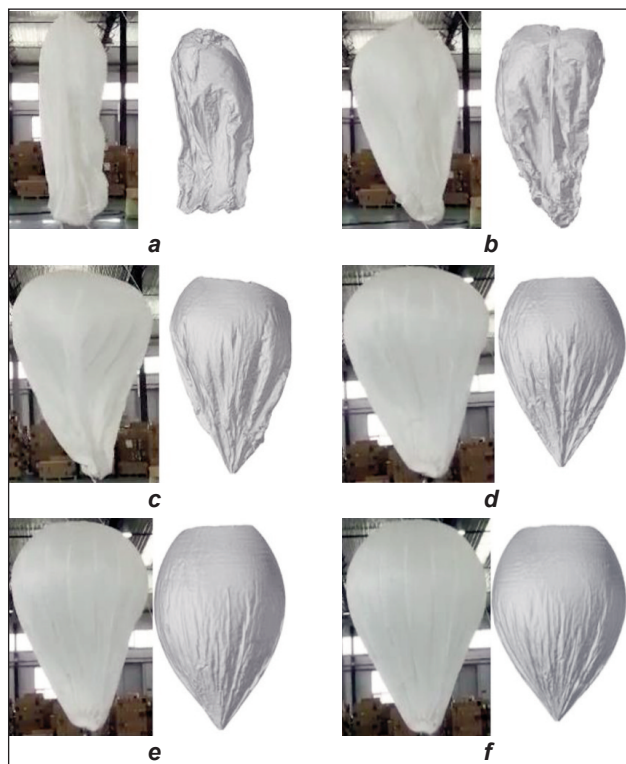

Fig. 7. Comparison of the maximum projected diameter

Fig. 6. Shape change comparison of numerical results and experimental results: *a* – *t* = 1 s; *b* – *t* = 2 s; *c* – *t* = 6 s; *d* – *t* = 10 s; *e* – *t* = 15 s; *f* – *t* = 20 s

Figure 7 shows the comparison of the maximum projected diameter. It also could be found that the change of shape is more violent in the initial and middle inflation stage and more stable in the final inflation stage. While the difference between the numerical and the experimental results are mainly caused by two aspects. On the one hand, there are some differences between the numerical model and the actual initial shape before inflation. On the other hand, the fixed constraints are used at the top and bottom, while the flexible constraints are used in experiment.
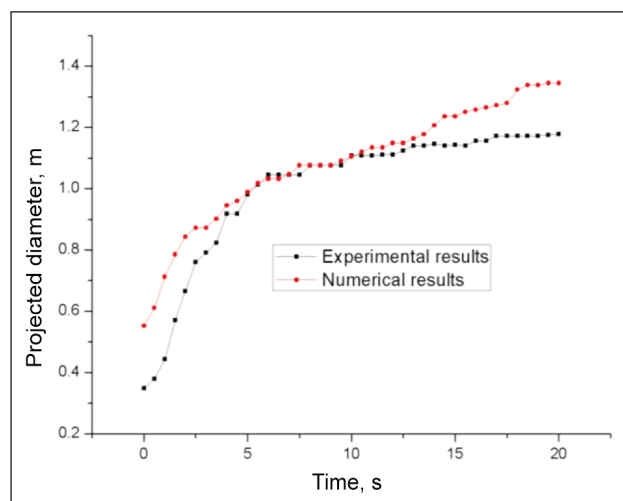
Figures 8 and 9 show the velocity vector and pressure contour of flow field during inflation.

Initial inflation stage (0-2s): Due to the asymmetric design of the internal airbag, the balloon partially expanded on one side (figure 8, *a*). The velocity of helium at the outlets is faster, while the density of helium is smaller than that of air. Therefore, there is no obvious high-pressure zone (figure 9, *a* and *c*), which has little effect on the outer skin far away from the internal airbag. Because the outer skin has not yet formed an effective constraint on the internal airbag, the point gas sources move with the displacement of the internal airbag. Furthermore, the displacement of the point gas sources aggravates the complexity of the flow field. The asymmetric flow field is obvious, and the balloon shows asymmetric expansion (figure 8, *b* and *c*).

Middle inflation stage (2-6s): The helium gathered at the top begins to flow to other unexpanded parts, and the balloon's top is further fully expanded. At the same time, the change of bottom is obviously affected by buoyancy. The bottom skin in the warp direction is almost completely expanded, while folds still exist in the weft direction (figure 8, *d* and *e*). Different
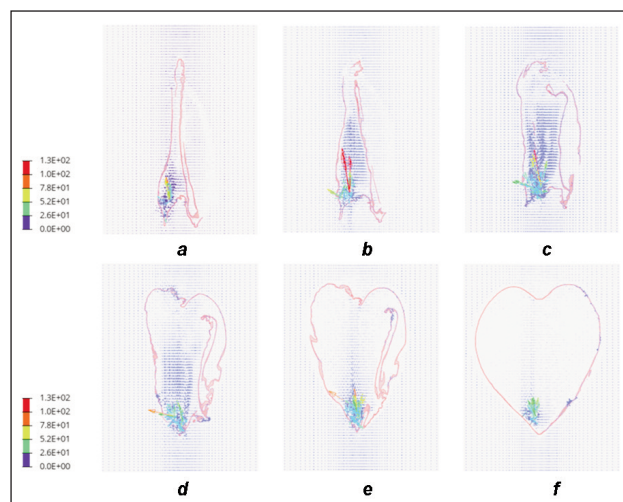

Fig. 8. Velocity vector of flow field: *a* – *t* = 0.1 s; *b* – *t* = 0.5 s; *c* – *t* = 1 s; *d* – *t* = 2 s; *e* – *t* = 6 s; *f* – *t* = 20 s

Fig. 9. Pressure contour of flow field: *a* – *t* = 0.1 s;
b – *t* = 0.5 s; *c* – *t* = 1 s; *d* – *t* = 2 s; *e* – *t* = 6 s; *f* – *t* = 20 s

Fig. 10. Effective stress contour of flow field: *a* – *t* = 0.1 s;
b – *t* = 0.5 s; *c* – *t* = 1 s; *d* – *t* = 2 s; *e* – *t* = 6 s; *f* – *t* = 20 s
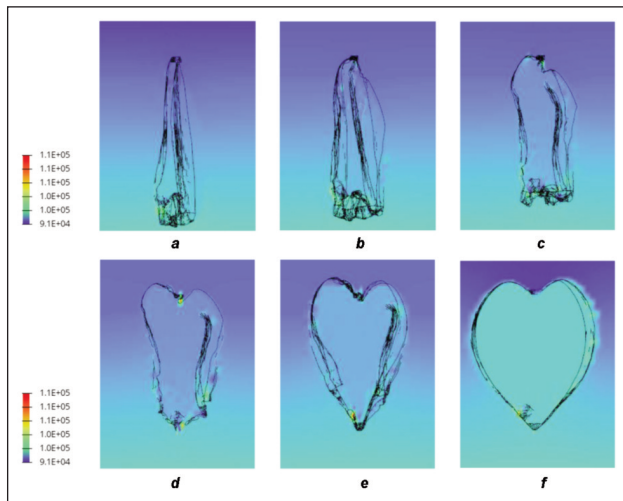
Fig. 11. Effective stress variety at different positions

from the initial inflation stage, the internal flow field in this stage is greatly affected by the constraints and folds. The internal flow field forms a high-pressure zone at the top and bottom (figure 9, *d*). The high-pressure zone at the top disappears with the expansion of the balloon (figure 9, *e*), while the bottom high-pressure zone constrained by the skin doesn't disappear.

Final inflation stage (6–20s): As the shape of the balloon gradually becomes symmetrical, the internal flow field changes more gently (figure 8, *f*). The stable position of the internal airbag also results in the formation of a stable high-pressure zone near the point gas sources (figure 9, *f*).

Figure 10 shows the effective stress contour. It can be found that the folds zones usually are stress concentration zones. The stress concentration disappears with the expansion of these folds. At the same time, the stress at the top and bottom of the balloon increases gradually with the increasing of buoyancy. Especially, the balloon's bottom affected by all the buoyancy generated by helium, and the stress concentration zone is the most obvious.

Figure 11 shows effective stress variety at different positions of the outer skin where the internal airbag is located. The impact of helium on the skin near the point gas sources (Element 57067) causes a sharp increase in stress. With the expansion of the balloon, the stress concentration decreases rapidly. However, the stress increases gradually with the increase of buoyancy. The stress at the top (Element 19783 and Element 17903) increases with the expansion of folds, and decrease after these folds fully expanded. Although the skin at the middle and lower parts (Element 19007 and Element 57656) expands first than that at the top, the skin at these parts slowly expands with the inflation of the balloon. Therefore, the stress of these parts changes gently.
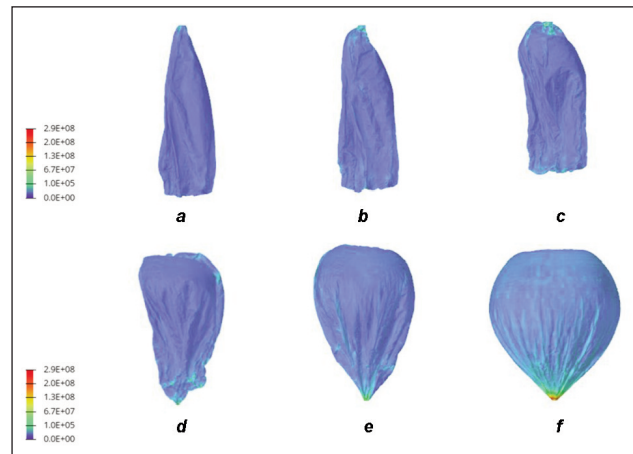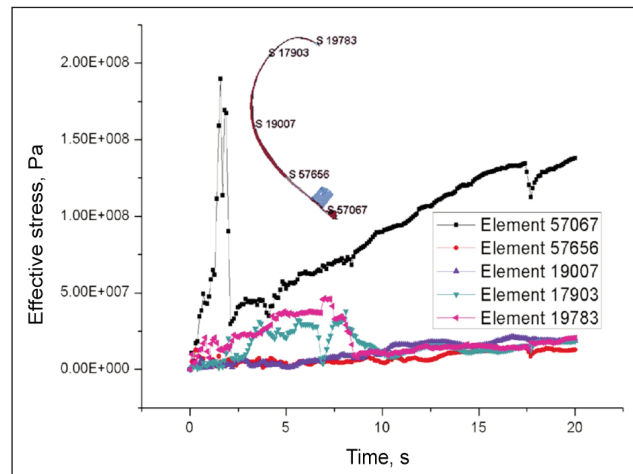
CONCLUSIONS

In order to study the mechanical mechanism of the core working process of rapid deployment aerostat, an air-launched balloon for rapid deployment was taken as the research object and the ground rapid inflation experiment and corresponding calculation were carried out. The rapid inflation process was calculated based on SALE method. The numerical results were in good agreement with the experimental results, which proved the feasibility and accuracy of the numerical method used in this work. The structure and flow field information of each stage which was difficult to obtain by experiments was obtained. The variation characteristics of the structure and flow field in each stage of the inflation process were summarized according the analysis of numerical results. The helium leakage phenomenon in the destructive inflation experiment was explained by stress analysis. The method proposed in this work can provide a reference for the design and optimization of rapid deployment aerostat in future.

REFERENCES

[1] Luo, X.L., Liu, J.T., Zhang, H.Y., Liang, K.Q., Zhang, F.Z., *General technology study of rapid deployment stratospheric aerostat*, In: Astronautical System Engineering Technology, 2019, 3, 5, 17–22 (in Chinese)

[2] Steinberg, S.Y., Holle, G.F., *Experimental results of the deployment/ rapid inflation characteristics of a buoyant Venus station balloon*, In: AIAA report, 1969, AIAA 1969–1017

[3] Andrew, S., Carten, J., Michael, R. W., *Air-Launched Balloon System Phase II Test Results*, In: Journal of Aircraft, 1982, 19, 8, 697–698, https://doi.org/10.2514/3.57452

[4] Andrew, S., Carten, J., Michael, R.W., *Parachute techniques employed in the Air-Launched Balloon System (ALBS) development program*, In: Journal of Aircraft, 1980, 17, 2, 65–66, https://doi.org/10.2514/3.57875

[5] Zhang, C.L., Chen, N.L., Geng, Y., *Study on preparation and mechanical behavior of high-density warp knitted aerostat envelope material*, In: Composites Science and Engineering, 2020, 9, 42–47 (in Chinese)

[6] Bessert, N., Frederich, O., *Nonlinear airship aeroelasticity*, In: Journal of Fluids and Structures, 2005, 21, 8, 731–742, https://doi.org/10.1016/j.jfluidstructs.2005.09.005

[7] Liu, J.M., Lu, C.J., Xue, L.P., *Investigation of airship aeroelasticity using fluid-structure interaction*, In: Journal of Hydrodynamics, Ser. B, 2008, 20, 2, 164–171, https://doi.org/10.1016/S1001-6058(08)60042-6

[8] Zhang, Y., Wang, X.L., *Fluid-structure interaction calculation framework for non-rigid airship based on explicit dynamics*, In: Journal of Shanghai Jiao Tong University, 2021, 55, 3, 311–319 (in Chinese), https://doi.org/10.16183/j.cnki.jsjtu.2019.351

[9] Stein, K.R., Benney, R.J., *Parachute inflation: a problem in aeroelasticity*, In: NASA-ADA 284375, 1994

[10] Tezduyar, T.E., Sathe, S., Schwaab, M., *Fluid–structure interaction modelling of ringsail parachutes*, In: Computational Mechanics, 2008, 43, 1, 133–142, https://doi.org/10.1007/s00466-008-0260-8

[11] Kim, Y.S., Peskin, C.S., *3-D parachute simulation by the immersed boundary method*, In: Computers & Fluids, 2009, 38, 1080–1090, https://doi.org/10.1016/j.compfluid.2008.11.002

[12] Gao, X.L., Zhang, Q.B., Tang, Q.G., *Numerical modeling of Mars supersonic disk-gap-band parachute inflation*, In: Advances in Space Research, 2016, 57, 11, 2259–2272, https://doi.org/10.1016/j.asr.2016.03.010

[13] Karagiozis, K., Kamakoti, R., Cirak, F., Pantano, C., *A computational study of supersonic disk-gap-band parachutes using Large-Eddy Simulation coupled to a structural Membrane*, In: Journal of Fluids and structures, 2011, 27, 2, 175–192, https://doi.org/10.1016/j.jfluidstructs.2010.11.007

[14] Cheng, H., Chen, C., Liu, X.H., Li, M., Chen, Z.C., Wei, L., *Numerical study of parachute inflation process based on smoothed particle hydrodynamics fluid structure interaction method*, In: Journal of Industrial Textiles, 2018, 47, 6, 1038–1059, https://doi.org/10.1177/1528083716661203

[15] Borker, R., Huang, D., Grimberg, S., Farhat, C., Avery, P., Rabinovitch, J., *Mesh adaptation framework for embedded boundary methods for computational fluid dynamics and fluid-structure interaction*, In: International Journal for Numerical Methods in Fluids, 2019, 90, 8, 389–424, https://doi.org/10.1002/fld.4728

[16] Liu, J.J., Long, J., Liang, K., Hou, J.D., Chen, Z.C., Cheng, H., *Reverse modeling of complicated fabric*, In: Journal of Industrial Textiles, 2016, 46, 2, 417–435, https://doi.org/10.1177/1528083715584140

[17] Souli, M., Ouahsine, A., Lewin, L., *ALE formulation for fluid-structure interaction problems*, In: Computer Methods in Applied Mechanics and Engineering, 2000, 190, 659–675, https://doi.org/10.1016/S0045-7825(99)00432-6

Authors:

PENG SUN[1], FEI LONG[2], HAN CHENG[1]

[1]Civil Aviation Flight University of China, Aviation Engineering Institute,
46 Nanchang road, 618307, Guanghan, China
e-mail: sunpeng_cafuc@126.com

[2]China Special Vehicle Research Institute,
8 Hangkong road, 448035, Jingmen, China
e-mail: longfei_605@126.com

Corresponding author:

HAN CHENG
e-mail: chenghanstorm@sina.com